Algal Research 95 (2026) 104614

Contents lists available at ScienceDirect

Algal Research

journal homepage: www.elsevier.com/locate/algal

Synthesis-dependent effects of silver nanoparticles on the green freshwater alga *Chlorella vulgaris*

Alzbeta Marcek Chorvatova [a,b,*], Martin Uherek [a], Anton Mateasik [a], Jaroslav Bruncko [a], Ildiko Matusikova [b], Jana Sedlakova-Kadukova [c,d]

[a] Department of Biophotonics, International Laser Center, Slovak Center of Scientific and Technical Information, Ilkovicova 3, 84104, Bratislava, Slovakia
[b] Faculty of Natural Sciences, University of Ss. Cyril and Methodius in Trnava, Nám. J. Herdu 2, 91701, Trnava, Slovakia
[c] ALGAJAS s.r.o., Prazska 16, 04011, Kosice, Slovakia
[d] Faculty of Forestry and Wood Sciences, Czech University of Life Sciences Prague, Kamycka 129, 16500, Praha 6, Suchdol, Czech Republic

ARTICLE INFO

Keywords:
Silver nanoparticles
Surface chemistry
Chlorella vulgaris
Endogenous fluorescence
Chlorophylls
NAD(P)H

ABSTRACT

Silver nanoparticles (AgNPs) synthesized by distinct routes differ in surface chemistry, which may reshape algal photophysiology and redox balance. The effect of biologically produced AgNPs (Agbio) was compared to chemically reduced citrate-capped AgNPs (Agchem), and/or to laser-ablated AgNPs (Agphys) on *Chlorella vulgaris* as a model organism to understand the nanoparticle effects in aquatic environments. UV–VIS absorption spectroscopy, spectrally resolved laser-scanning confocal microscopy of red chlorophyll fluorescence, chlorophyll fluorescence-lifetime imaging (FLIM), flavin autofluorescence imaging, and time-correlated single-photon counting (TCSPC) of NAD(*P*)H were combined to resolve their effects, while scanning electron microscopy provided morphological context. The absorption maxima appeared at 407 nm, 410 nm, and 412 nm for Agphys, Agbio, and Agchem, respectively. Agbio produced the strongest suppression of red chlorophyll fluorescence peaking at 680 nm. FLIM recorded with a BP of 700 ± 20 nm, following excitation by a 445 nm ps laser, uncovered specific dynamics over 7 days. Flavin fluorescence, monitored between 483 and 632 nm, rose immediately for Agchem/Agphys but became significant only at Day 7 for Agbio. NAD(*P*)H fluorescence lifetimes recorded by TCSPC at 420–680 nm (405 nm excitation) revealed an acute drop in NAD(*P*)H photon counts at Day 1 and a universal increase of Tau1; Tau2 rose persistently for Agbio, increased transiently for Agphys, and showed no sustained elevation for Agchem. The data support a two-phase redox response – early compensation followed by particle-dependent depletion or re-equilibration - and indicate a phototoxicity ranking Agbio > Agchem ≈ Agphys under our exposure conditions. Gathered results show that the synthesis route is a primary determinant of algal responses.

1. Introduction

Currently, research across various fields has increasingly focused on nanotechnology due to its versatile potential to address urgent global challenges. Nanomaterials possess unique characteristics that enhance efficiency, improve applicability, and support environmental and economic sustainability [1]. The application of various nanoparticles (NPs) in commercial products and industrial processes has expanded considerably, and their use is expected to continue growing, including silver nanoparticles (Ag NPs). An extensive literature is now available regarding the AgNPs' properties [reviewed in [2]], potential mechanisms of action [3], as well as key influencing factors and toxicity [4]. However, several knowledge gaps persist regarding NP applications, necessitating further research to assess their distribution, accumulation, and long-term effects on biological systems based on the NPs production routes. The environmental and health effects of NPs on non-target organisms, including soil and aquatic microorganisms, remain largely unexplained [5].

Size and shape were initially considered the primary factors responsible for the toxicity of AgNPs [6]. Different sizes of the NP types were demonstrated to affect cellular uptake [7] and biological activity [4,8]. However, subsequent research revealed that the “corona” formed on NP surfaces based on their production route or upon exposure to biological environments strongly influence their biological activity

* Corresponding author at: International Laser Center, Slovak Center of Scientific and Technical Information, Ilkovicova 3, 84104, Bratislava, Slovakia.
E-mail address: Alzbeta.MarcekChorvatova@cvtisr.sk (A. Marcek Chorvatova).

https://doi.org/10.1016/j.algal.2026.104614
Received 20 October 2025; Received in revised form 10 February 2026; Accepted 24 February 2026
Available online 25 February 2026

[9,10]. This complexity highlights the importance of understanding how different synthesis approaches may influence NP properties and behavior within various ecosystem components.

Traditional NP synthesis methods, which are predominantly based on chemical or physical approaches, suffer from several limitations. The most critical issues include low stability, high energy consumption, and, in the case of chemical routes, the necessity of using toxic chemicals and generating harmful waste. Moreover, low biocompatibility is frequently observed [11,12]. In contrast, biological approaches have gained increasing attention over the past two decades. Numerous studies confirmed that different organisms, their extracts, or even spent cultivation media can be utilized for NP production, as reviewed elsewhere [13–15]. Environmental sustainability and simplified synthesis methods represent the greatest advantages of biological approaches; however, this production route also has limitations, including variation in shape and size, difficulties in scaling up, and long-term stability issues due to deterioration of capping agents such as proteins or polysaccharides [16].

Given the vast diversity of organisms and bioactive molecules, numerous possibilities exist for their utilisation in NP production, as evidenced by the growing number of published studies. However, the relationship between biological production routes and the characteristics of produced NPs compared to other production methods remains underexplored. Only a few studies have attempted to understand the differences directly related to NP synthesis methods. For example, [5] reviewed the specific biological activities, namely anticancer, antimicrobial, and antioxidant properties, of NPs prepared using plant extracts, while [17] compared the antibacterial activity of chemically and biologically prepared silver NPs.

Recent advancements in biological methods, including our previous work on biologically produced AgNPs prepared with aqueous extracts of *Parachlorella kessleri* (*P. kessleri*) [18–20], demonstrate their great potential, not only due to their environmentally sustainable synthesis but also because of the specific characteristics of the produced NPs.

The aim of the study is to apply advanced biophotonics methods to compare the effect of differently produced AgNPs on endogenous fluorescence and cellular redox balance in the model green alga *Chlorella vulgaris* (*C. vulgaris*). Namely, the effects of biologically produced AgNPs (Agbio), chemically reduced citrate-capped AgNPs (Agchem), and laser-ablated polydisperse AgNPs (Agphys) are studied using confocal microscopy and time-resolved fluorescence techniques to elucidate the synthesis-specific responses that conventional bulk assays cannot resolve.

2. Material and methods

2.1. Preparation of silver NPs

2.1.1. Biological approach

Biologically synthesized AgNPs were prepared using aqueous extracts of *P. kessleri* biomass, as previously described [18–20]. Briefly, 1 g of dry algal biomass was boiled in 200 mL of distilled water for 20 min. The extract was filtered (0.22 μm) and an $AgNO_3$ solution was added to the extract to achieve a final silver concentration of 100 mg/l. The complete synthesis protocol and physicochemical characterization (UV–Vis, FT-IR, TEM, EDS) of biologically prepared AgNP were previously published [18,19]. For the present study, batch-to-batch consistency was verified by UV–Vis spectrophotometry to ensure reproducibility of particle properties.

2.1.2. Chemical approach

Chemically reduced citrate-capped AgNPs (Agchem) were synthesized by the citrate reduction method [21]. A 100 mg/l $AgNO_3$ solution (50 ml) was brought to boiling in a water bath. At the first sign of boiling, 1 ml of 1% (*w/v*) sodium citrate solution was added. A reflux condenser was attached to the flask, and the contents were boiled for 1 h [21]. The resulting colloidal suspension was cooled to room temperature. The final silver concentration after reduction was 100 mg/l.

2.1.3. Physical approach

Laser-ablated polydisperse AgNPs (Agphys) were prepared by the method of pulsed laser ablation in liquid [22]. The solid-state Nd:YAG pulsed laser (Quanta Ray Pro 250 working at 1064 nm, 20 ns pulse length, 10 Hz pulse repetition rate, and energy approximately 80 mJ per pulse) was used for the ablation of the metal target in deionized water (without any surfactant application). The metal target was submerged in the glass beaker approx. 10 mm under the water level, and the water volume for the resulting colloid was 15 ml. The laser beam was focused at the target surface with an energy fluency ~1.5 $J.cm^{-2}$. The process was applied for 10 min. The resulting AgNP suspension was stored at 4 °C and used within 2 weeks.

2.2. Assaying biological effects of NPs on alga C. vulgaris

The effects of prepared NPs were studied using the live culture of freshwater green microscopic alga *C. vulgaris* strain 262 GAFFRON/SAG 211-1e. Alga were purchased from CCALA collection of the Institute of Botany, Czech Academy of Sciences, Czech Republic Alga were cultivated in MillieuBristol medium [23] In the first 4–5 weeks, algae were placed in the cultivation room under 6 fluorescent lamps, each 18 W, 4100 K, 1850 Lm, positioned 30 cm above the culture flasks at 21 °C under a 12:12 h light/dark photoperiod. From the week 5–6, the algae were kept at the room temperature (22–23 °C) under 20 W LED light WRB with luminosity 1730 lm and 12:12 light/dark conditions. The NPs were added to algae between week 8–10 after inoculation, corresponding to exponential phase, at the initial cell density around 3000–4000 cells/μl [= 3–4 × 10^6 cells ml^{-1}] (D0).

For exposure experiments, cultures in the exponential growth phase were used (weeks 8–11). All NPs were stored at 4 °C before their usage in the experiments. A volume of 250 μl of each AgNPs suspension was added to 1 ml of algal culture at Day 0 (D0) in 1.5 ml Eppendorf tubes without additional dispersion treatment. In the control conditions, 250 μl of distilled water was added. With a final silver concentration after production of 100 mg/l, the estimated silver concentration in the tested samples was 20 mg/l. The measurements were then taken at Day 1 (D1) (acute response) and Day 7 (D7) (chronic response) post-exposure. This approach was repeated 3 times, representing 3 independent biological replicates. AgNP stability and potential aggregation in culture medium during the 7-day exposure period were monitored by analysis of confocal microscopy images, and no aggregation or change in the sample transparency was observed between D1 and D7.

2.3. Analytical methods

2.3.1. Absorption measurements

Absorption spectra of the alga were recorded by UV–Visible Spectrometer CARY 50 Bio (Varian, USA) in the spectral range 300–800 nm.

2.3.2. Confocal microscopy measurements

Laser scanning confocal microscopy (LSCM) images were acquired using an Axiovert 200 LSM 510 Meta microscope (Carl Zeiss, Germany), equipped with a C-Apochromat 40×/1.2 NA water immersion objective, as described previously [24,25]. Excitation was performed with a 450 nm single-mode laser diode (Kvant, Slovakia), and fluorescent emission was detected using an internal photomultiplier or spectral META detector. The two- channel imaging setup was: Channel 1, recorded with a BP 500–550 nm bandpass filter, served to monitor the flavin fluorescence, while channel 2, using a BP 650–710 nm filter, recorded the endogenous red chlorophyll fluorescence of the *C. vulgaris* alga, peaking at 680 nm, as previously reported [24]. Maximal laser power density for the 450 nm laser line, used for the sample excitation, was 1580 Wm^{-2}. Spectrally resolved images were acquired using the META detector with

an 11 nm step from 613 to 713 nm to record the red chlorophyll spectra, or from 483 to 632 nm to cover the green spectral region (mostly flavin fluorescence).

2.3.3. FLIM measurements

Fluorescence lifetime imaging microscopy (FLIM) gathered images using a 445 nm picosecond laser diode (BDS-SM-445-FBC, Becker&Hickl, Germany, 20 MHz repetition rate), reflected to the sample via an epifluorescence path of the inverted Axiovert 200 LSM 510 Meta microscope (Carl Zeiss, Germany) with C-Apochromat 40×, 1.2 NA, as previously described [24]. Fluorescence emission passing through a BP 700 ± 20 nm bandpass filter was detected by a PMC-100-20 photomultiplier (Becker&Hickl GmbH, Germany) coupled to an SPC-830 TCSPC board (Becker&Hickl GmbH, Germany).

2.3.4. TCSPC measurements

NAD(*P*)H fluorescence lifetimes were recorded by time-correlated single photon counting (TSCPC), employing a 405 nm picosecond laser diode (BDS-SM-405-FBC, Becker&Hickl, Germany) as an excitation source (20 MHz repetition rate, ~1 mW average output power). Samples were placed in a UV-proof quartz cuvette (1 ml sample volume). The fluorescence emission was collected through a 450 ± 20 nm bandpass filter (FB450–40, Thorlabs) and detected by 2 perpendicular photomultipliers (HPM-100-40, Becker&Hickl GmbH, Germany) in L-format geometry to minimize scattering artifacts.

2.3.5. SEM measurements

Scanning electron microscope (SEM) images were acquired using a LEO 1550 field emission SEM (Carl Zeiss, Germany) operating in InLens imaging mode at EHT 3 kV acceleration voltage and 50,000× magnification, as previously described [26]. The samples for SEM measurements were prepared by dropping the AgNPs solution on a silicon wafer and dried at room temperature. The standard microscope mount was used.

2.4. Data analysis

Data analysis was done as previously described [24,25]. ZEN 2011 software (Zeiss, Germany) or home-built procedures were employed to analyze LSCM images. Effects on endogenous fluorescence of *C. vulgaris* were evaluated from multichannel and/or spectrally resolved confocal images by comparing the intensities captured in the detection channels covering the green and red regions of the visible spectrum. For numerical comparison, the mean fluorescence intensities of the individual *C. vulgaris* bodies visible in confocal images for each channel were calculated as shown in Figs. 2 and 5. The fluorescence intensity of each of the cell body was determined by averaging the fluorescence signal from image pixels belonging to the given body. The body's pixels were determined autonomously using an image segmentation technique. The segmentation procedure was based on the generation of a binary mask, derived from an image that was created by summing all available channels into a single grayscale image. From this summed image, a binary mask was computed using Otsu's thresholding method [27], which automatically determines the optimal threshold value by maximizing inter-class variance. This binary mask was subsequently utilized to extract intensity profiles separately for cell pixels and background pixels. The resulting profiles were normalized by averaging across the number of pixels from which they were obtained.

Measured FLIM images were segmented before decay analysis to delineate boundaries and pixels belonging to each cell body similarly as was done for confocal images. Final summed decay signals from each *C. vulgaris* were analyzed with a two component multi-exponential model separately for each cell object in the image and results were presented as average values from all the *C. vulgaris* bodies found in the image. The calculations were done using a custom Python script, employing the least squares method from the SciPy library. As an instrument response function in the data fitting procedure, the synthetic IRF function produced by SPCImage software (Becker Hickl, Germany) was used. Only the first scan was used to avoid artifacts induced by photobleaching. FLIM images at Fig. 4 and TCSPC recordings at Figs. 6 and 7 were processed using the proprietary software package SPCImage 8.4 NG (Becker&Hickl, Germany). NADPH decays were evaluated as a 2-exponential decay, while NADPH photon counts corresponded to total integrated counts.

Figures were generated by Origin 6.0 Professional. Statistical comparison was performed using a one-way ANOVA test; data gathered in the presence of AgNPs were compared to control conditions, with $^{*}p < 0.05$ considered as significant vs. control in D1 and $\#p < 0.05$ considered as significant vs. control in D7. In graphs, mean ± SEM (standard error of mean) is presented.

3. Results

Our research aim is to compare the biological effects of AgNPs produced by different routes on a model aquatic organism, the microscopic green freshwater alga *C. vulgaris*. Three synthesis routes were employed: a biological route using biomass of the alga *P. kessleri*, a chemical approach using natrium citrate, and a physical approach using laser ablation of metal discs. A set of complementary techniques was used to deliver an integrated view – optical, functional, metabolic, and ultrastructural - of how AgNPs produced by different synthesis routes influence biological systems. In this study, a concentration of 20 mg/L of AgNPs was chosen to mimic high concentrations found in polluted areas [28] and to elicit a clear response from the studied system.

3.1. Absorption measurements

UV-VIS absorption spectroscopy offers a rapid, non-invasive means of characterising both the optical impact of NPs exposure on photosynthetic organisms and the physicochemical properties of the particles themselves. We therefore collected the full absorption spectra (300–800 nm) for the three AgNPs preparations, Agphys, Agbio, and Agchem, and estimated their size and distribution (Fig. 1 top left).

The absorption maxima appeared at 407 nm for Agphys, 410 nm for Agbio, and 412 nm for Agchem. These closely spaced maxima indicate comparable core sizes of the NPs [29,30]. Peak-width, however, suggested pronounced differences in polydispersity. The narrowest distribution of NPs (according to the width of the spectrum distribution) was observed for Agchem and Agphys. Agbio has a larger distribution, with the spectral shoulder toward 500 nm that points to the occurrence of some larger NPs. The smooth, symmetrical line shapes without secondary resonances further suggest predominantly spherical morphologies [31].

Cell-surface morphology and NP architecture were visualized using SEM (Fig. 1 top right and bottom). Gathered images allowed estimation of the NPs' size: smaller NPs were estimated for Agbio (around 10–20 nm, Fig. 1 top right), when compared to Agchem and Agphys (Fig. 1 bottom), which presented particle sizes around 40 nm (30–45 nm).

3.2. Chlorophyll fluorescence

Next, the biological effects of the differently produced AgNPs were evaluated. The alga *C. vulgaris* was chosen as a model organism for the evaluation of the effect of differently produced AgNPs on the aquatic ecosystem, a very common alga in the freshwater environment.

First, we have tested the effect of produced AgNPs on the algal chlorophylls by means of their endogenous fluorescence [24]. Red chlorophyll fluorescence was recorded by LSCM in the spectral region 650–710 nm (Fig. 2A) to gather fluorescence close to the chlorophyll maximum at 680 nm (see spectrum at Fig. 3Ba). We have observed significantly reduced chlorophyll fluorescence of the alga *C. vulgaris* by Agbio, and, to a lesser extent, also by Agphys and Agchem (Fig. 2B).

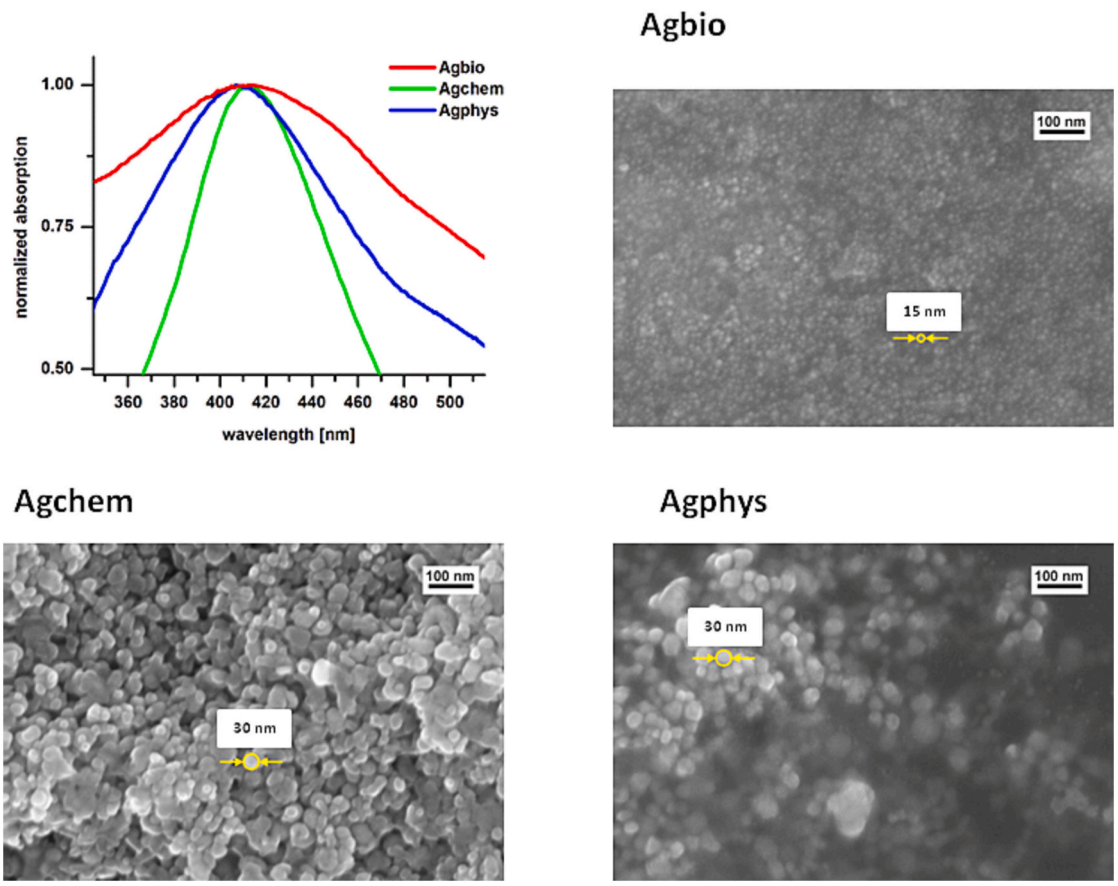

Fig. 1. Absorption spectra and SEM images of the AgNPs. Top left) Absorbance recorded by UV-VIS Spectrometer in the spectral range 300–800 nm. Top right and bottom) SEM examples of differently produced AgNPs on the Si substrate, including an example of particle size measurement.

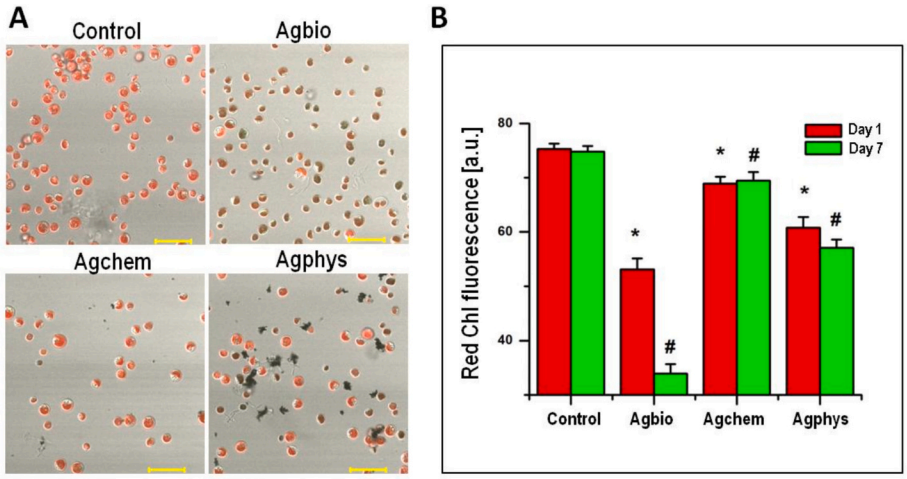

Fig. 2. Red chlorophyll fluorescence. A) Recording by LSCM on 2 channels (illustrated images at D7) took place with the following setup: channel 1, recorded with BP 500–550 nm, served to monitor the green fluorescence (analysis at Fig. 5), while channel 2, using BP 650–710 nm filter, recorded the red chlorophyll fluorescence. Overlay of channels, including the transmission channel, is shown. Scale bars represent 20 μm. B) Effect of AgNPs on the red fluorescence, calculated from channel 2. $^{*}p < 0.05$ vs. control in D1, #p < 0.05 vs. control in D7 (12–16 N^{o} of samples). (For interpretation of the references to colour in this figure legend, the reader is referred to the web version of this article.)

To better understand the observed reduced red chlorophyll fluorescence by AgNPs, we have also evaluated their effect on the chlorophyll spectra determined by spectrally-resolved confocal microscopy. Original spectrally-resolved images are shown in Fig. 3A, while normalized spectra are illustrated in Fig. 3B. The spectral maximum remained unchanged in all conditions at 680 nm, as expected for chlorophylls [24]. The spectral shape remained unchanged in all but Agbio conditions. Observed change in the latter case can be related to the reduced red chlorophyll intensity in the presence of Agbio in these conditions (as demonstrated in Fig. 2B). At the same time, observed decrease in the chlorophyll fluorescence (Agbio, Agchem, Agphys) without change in their fluorescence emission spectral maxima indicates chlorophyll

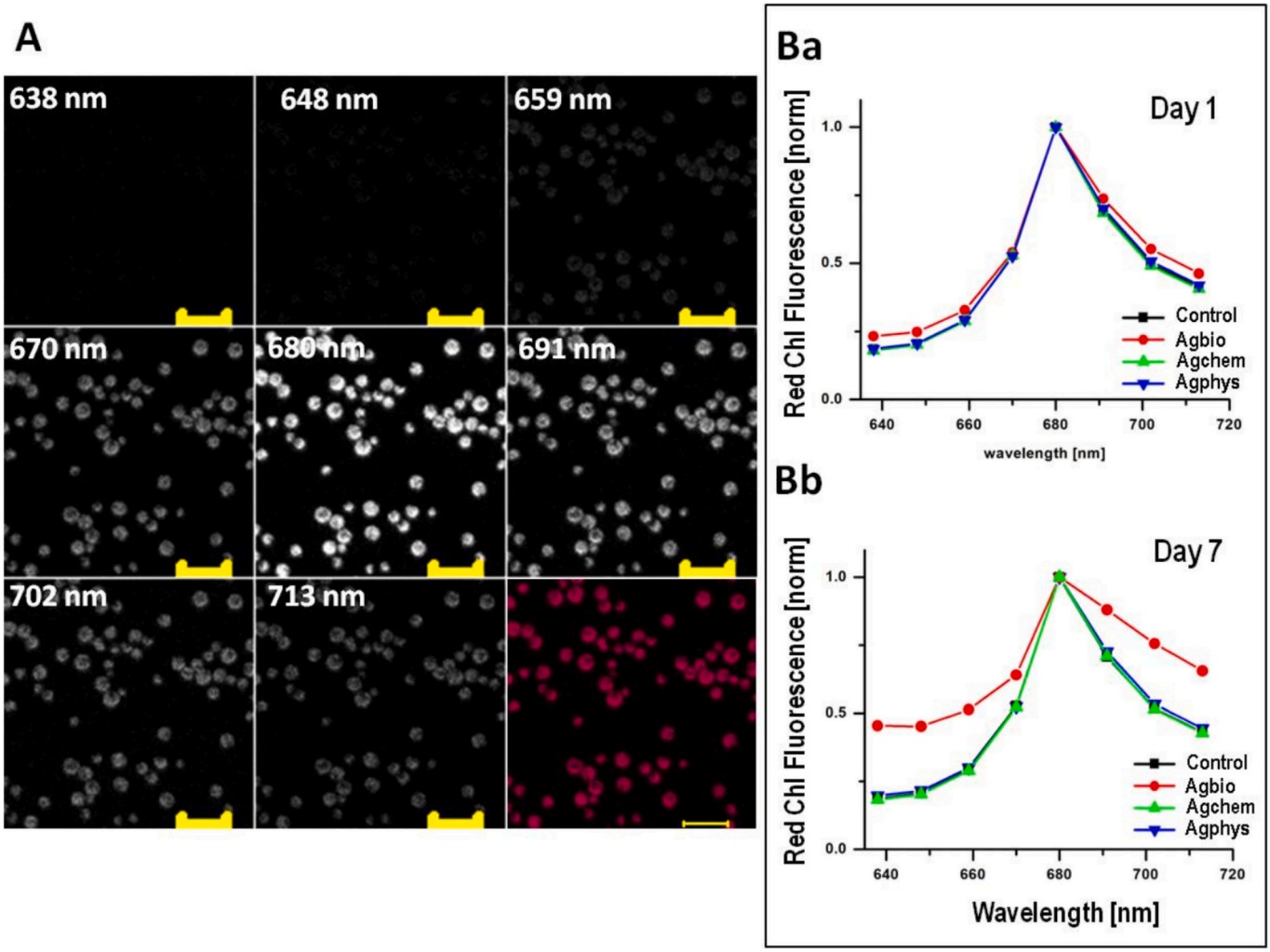

Fig. 3. Spectrally-resolved confocal microscopy measurements of the red chlorophyll fluorescence of alga *C. vulgaris*. A) Fluorescence images of endogenous fluorescence of *C. vulgaris* alga gathered by excitation at 450 nm with 11 nm step between 638 and 713 nm (lambda scan on the left with red composite image is shown, scale: 20 μm). B) Normalized spectra after D1 exposure (a) and after D7 exposure (b) (11–14 N° of samples). (For interpretation of the references to colour in this figure legend, the reader is referred to the web version of this article.)

fluorescence quenching by enhanced non-radiative energy dissipation (e.g., via ROS or heat) [32].

To further investigate the effect of the AgNPs on the chlorophyll fluorescence, we have also evaluated its fluorescence lifetimes, recorded by FLIM (Fig. 4), which indicate changes in the molecular environment of the chlorophyll molecules. Clear shortening of the chlorophyll fluorescence lifetimes was observed in the presence of Agbio. This effect was observable already after D1, but was even more pronounced at D7 (Fig. 4B). It can explain the reduced chlorophyll fluorescence recorded in Fig. 2. On the other hand, Agchem and Agphys induced a prolongation of the fluorescence lifetimes at D1, suggesting a compensatory adjustment in the excited-state dynamics of chlorophyll molecules in response to the decrease in chlorophyll fluorescence. At D7, no change in the presence of Agchem and a smaller, but significant shortening of the fluorescence lifetimes induced by Agphys indicate that a separate mechanism is likely put in place in these conditions. It is also noteworthy that, as illustrated in Fig. 4A, while in the case of Agbio nearly all cells exhibited shortened fluorescence lifetime, no difference was observed in the case of Agchem. In the presence of Agphys, as illustrated by red in Fig. 4A., 2 distinct fractions of cells exhibiting altered photophysical properties were noted.

Data suggest that the Agbio particles inflict functional PSII impairment, leading to a uniform, progressive cell death and fluorescence lifetime shortening (Fig. 4A). Citrate-capped particles were associated with a prolongation of chlorophyll fluorescence lifetimes (Fig. 4B), initially close PSII reaction centres faster than protective non-photochemical quenching (NPQ) can respond, so excitons persist longer (lifetime prolongation), as previously reported for NP-induced stress in photosynthetic organisms [32]. By D7, the average fluorescence lifetime in the Agchem treatment returned to values comparable to the control, suggesting a recovery of photoprotective energy dissipation rather than irreversible PSII damage. In contrast, the highly polydisperse, ligand-free Agphys particles elicited a heterogeneous response: maintained or recovered normal lifetimes, while others showed signs of severe stress or cell death, possibly related to particle aggregation or internalisation (seen as dark clusters in Fig. 2A). Although these particles activate strong photoprotection (NPQ), the population-average drops at D7 yet remains above the Agbio level.

3.3. *Flavin fluorescence*

Flavin fluorescence is related to the functioning of the flavin complexes in algal cells, and reports the redox state of mitochondrial flavoproteins [33,82]. Images of the laser-scanning confocal micrographs reveal that the oxidative shift is not uniform across the culture. In the case of Agbio, a minority of cells exhibit very bright flavin signals (single

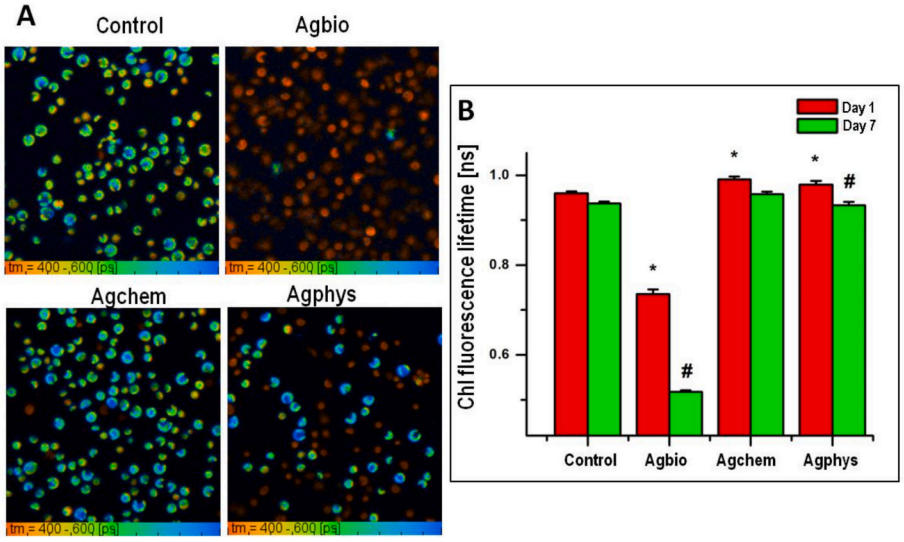

Fig. 4. FLIM images of chlorophyll fluorescence of *C. vulgaris*. A) Original FLIM images were gathered following excitation by a 445 nm ps laser, BP 700 ± 20 nm; lifetime distribution at D7 is shown in the 400–600 ps range (red-blue). B) Statistical analysis for the mean fluorescence lifetime,*$p < 0.05$ vs. control in D1, #p < 0.05 vs. control in D7 (500–1000 N^o of cells). (For interpretation of the references to colour in this figure legend, the reader is referred to the web version of this article.)

hyper-fluorescent cell). On the other hand, Agchem and Agphys elicited a more widespread, moderate increase (Fig. 5A). The blue clusters in the Agphys field correspond to the reflection on agglomerated, laser-ablated particles adhering to the cell surface, possibly corresponding to the surface-driven generation of reactive oxygen species (ROS) [34,35].

The corresponding data (Fig. 5B) indicate a NP-dependent, time-progressive oxidation of intracellular flavins in *C. vulgaris*. All three AgNPs formulations elevated green flavin fluorescence relative to the control. Significant fluorescence increase was observed primarily for Agchem and Agphys, suggesting that the electron transport is impaired, or that they trigger an immediate, surface-driven oxidative burst. The significant rise of this fluorescence at D1 ($p < 0.05$) is further intensified by D7, possibly implying a rapid onset of mitochondrial oxidative stress driven by extracellular Ag^+ and/or ROS release [36]. In contrast, Agbio exhibits no significant change on D1, yet reaches significance by D7. This possibly suggests a slower transition to an oxidized redox state as cellular antioxidant reserves became depleted.

3.4. NAD(P)H fluorescence

Flavin fluorescence is an important indicator of the redox properties in the cells [37] and is often directly related to the production of NAD(*P*)H. In the alga, the main source of this fluorescence is an NADPH-related fluorescence [38]. For that reason, in the next step, we have recorded NAD(*P*)H fluorescence in algae. We have employed TSCPC to also evaluate changes in the fluorescence lifetimes and their amplitudes to track red/ox properties of the cells.

All AgNPs variants decreased the NAD(*P*)H fluorescence on D1 (Fig. 6A), suggesting a rapid consumption of NADPH reducing equivalents to combat ROS. The significant decrease in the photon counts in all conditions is in agreement with the rise in the flavin fluorescence (Fig. 5B) and with the decrease in the red chlorophyll fluorescence (Fig. 2B). Lower values of photon counts may correspond to a smaller NADPH pool (or stronger dynamic quenching by ROS) and reflect the depletion rate descending with (Agchem = Agphys) > Agbio. By D7, cells exposed to Agchem and Agphys partially replenish NADPH yet remain below control, suggesting continued - but mitigated - oxidative

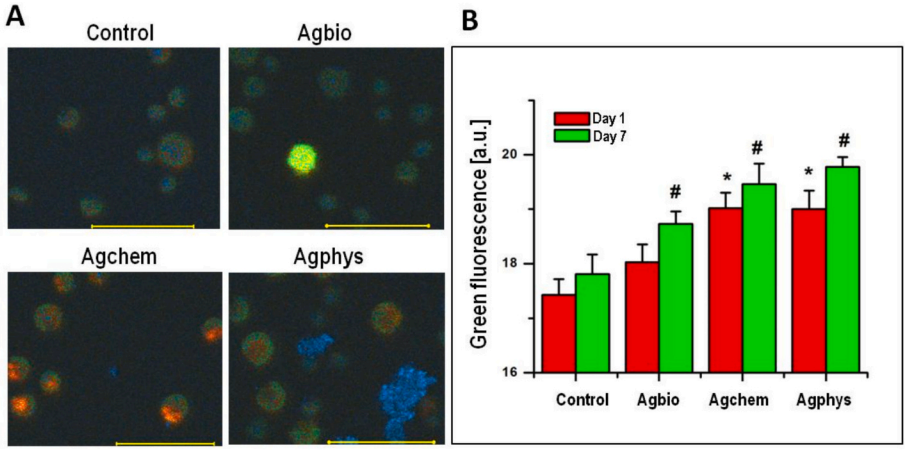

Fig. 5. Spectrally-resolved confocal microscopy of *C. vulgaris* alga green fluorescence. A) Fluorescence images gathered at D7 by excitation at 450 nm with 11 nm step between 483 and 632 nm (composite image from 483 to 611 nm is shown, scale: 20 μm). B) Statistical analysis is calculated from channel 1, recorded with BP 500–550 nm (12–16 N^o of samples). *$p < 0.05$ vs. control in D1, #p < 0.05 vs. control in D7. (For interpretation of the references to colour in this figure legend, the reader is referred to the web version of this article.)

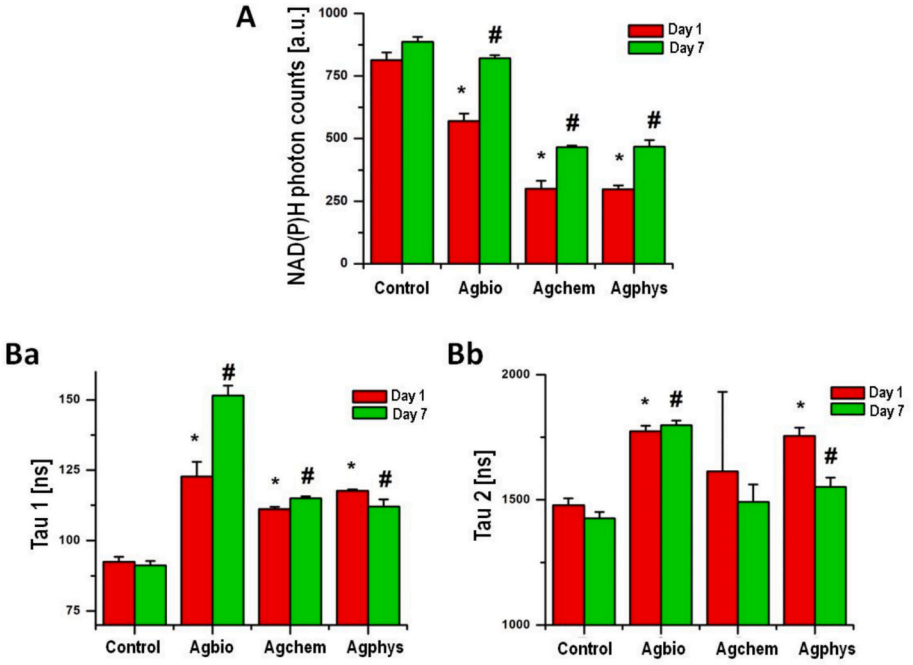

Fig. 6. NAD(*P*)H fluorescence lifetimes. A) Photon counts corresponding to the fluorescence intensity and B) fluorescence lifetimes Tau 1 (a) and Tau 1 (b) of the NAD(*P*)H fluorescence, recorded by TCSPC after excitation at 405 nm and emission between 420 and 680 nm (7–12 N° of samples).

demand. Agbio particles cause a smaller initial depletion and notable partial rebound, implying early mobilisation of alternative reductive pathways (Fig. 6A).

Under the recorded conditions, the NAD(*P*)H photon counts' decrease was accompanied by the prolongation of the fluorescence lifetime components, specifically Tau1 and Tau2 (Fig. 6B), indicating alterations in the cellular redox state and metabolic dynamics in response to the presence of different AgNPs. Values of increasing Tau1 (shift of free NAD(*P*)H toward more viscous / protein-crowded domains) upon exposure to NPs (Fig. 6Ba) indicate elevated oxidative stress and metabolic slowdown, most prevalent upon exposure to Agbio by D7 [39,40]. Pronounced, sustained high levels of Tau2 values in the presence of AgNPs (Fig. 6Bb) reflect a tighter, less quenched binding of NAD(*P*)H, possibly due to an engagement of NADPH-dependent repair enzymes to oxidoreductases upon exposure of Agbio and also Agphys (Fig. 6). This observation is also in agreement with more NADPH presence, regarding longer fluorescence lifetimes of NADPH (close to 4.4 ns) when compared to the NADH ones [41].

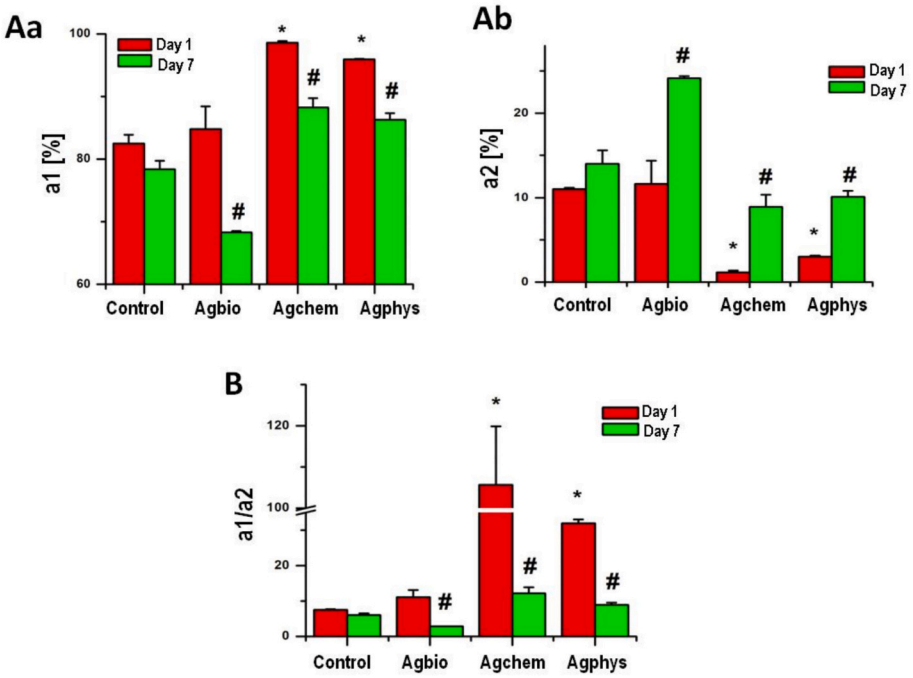

Fig. 7. NAD(*P*)H fluorescence lifetime amplitudes. A) Amplitude a1, corresponding to NAD(*P*)H lifetime Tau 1 (a) and amplitude a2 to that of Tau 2 (b) and B) a1/a2 ratio, recorded by TCSPC after excitation at 405 nm and emitted between 420 and 680 nm (7–12 N° of samples).

Next, changes in the a1 (short lifetime) and a2 (long lifetime) amplitudes of the NAD(*P*)H lifetimes (corresponding to "free" and "bound" NAD(*P*)H, respectively) were recorded (Fig. 7A). Stable NADPH fluorescence over time suggests that the cellular metabolism or redox state remains unchanged without external intervention. However, application of Agchem and Agphys NPs significantly elevated the a1/a2 ratio at D1 (Fig. 7B), suggesting a rapid shift toward a more oxidized cellular state, which could reflect enhanced oxidative stress, alterations in metabolic activity, and/or changes in the cellular redox balance [42]. In the presence of Agbio, no significant change was noted at D1. By D7, a decrease in the a1 amplitude, accompanied by an increase in the a2, leads to a reduced a1/a2 ratio under this condition. Conversely, for Agchem and Agphys, we observed a notable increase in a1 coupled with a decrease in a2, leading to an elevated a1/a2 ratio. An increase in the a1 component has been linked to enhanced NAD(*P*)H production or a shift toward a more oxidized state and/or higher NAD(*P*)H consumption during the oxidative stress process [43,44]. In contrast, an increase in a2 (notably in Agbio) may reflect higher levels of reduced NAD(*P*)H [43]. Additionally, near-zero a2 values in the case of Agchem (especially at D1) may account for the high mean standard error values for Tau2 in this condition, indicating greater variability in the measured fluorescence lifetime. Thus, the order of reductive-capacity exhaustion is Agchem > Agphys > Agbio, with Agbio inducing sustained oxidative pressure over several days (indicative of stress response) yet eliciting the greatest mobilisation of bound (reduced) NAD(*P*)H [43,45].

4. Discussion

Gathered results demonstrate a differential mechanism of action induced by AgNPs on alga *C. vulgaris,* based on the origins of their production. Biologically produced Agbio affected the chlorophylls primarily, inducing a chlorophyll fluorescence intensity reduction that was associated with the shortening of their fluorescence lifetimes. On the other hand, chemically and physically produced Agchem and Agphys rather acted on algal metabolism, as evidenced by their action on flavin and NAD(*P*)H fluorescence. Chemical synthesis yielded the most uniform AgNPs; conversely, physical and biological routes produced broader size distributions with occasional larger entities. Variations in the toxicity of AgNPs produced by biological, chemical, and/or physical approaches appear to be associated with their surface characteristics (e.g., surface charge, coating, and/or corona composition) [10,46]. Biologically produced AgNPs are coated with a protein-rich corona that affects their cellular interactions and toxicity [18,19,47]. Chemically produced AgNPs have a citrate coating, as sodium citrate was used for their production, while physically produced AgNPs lacked any corona [48].

Based on our previous results, it is evident that the preparation method and choice of organism used during synthesis significantly affect the physical and chemical properties of the resulting NPs. Remarkably, the differences in NPs production routes also affect purely chemical or physical processes. For example, improved characteristics have been observed for indium-containing NPs when produced through biological routes. The electrical sensitivity of gas sensors containing biologically produced In_2O_3 NPs was significantly higher compared to those synthesized using traditional methods [49]. Similarly, photocatalytic hydrogen production rates increased threefold when indium sulfide NPs synthesized with biological agents were used instead of those synthesized without biological agents [50]. Chemical synthesis methods typically produce smaller [51–53], more monodisperse [52,54], and more stable [4,52,55] AgNPs. Biological synthesis methods often result in larger, polydisperse particles, but smaller and very stable particles also can be obtained after optimization of conditions [56–58]. In our case, we have also observed high dispersion in the size distribution of Agbio particles (Fig. 1A), with predominant smaller sizes (Fig. 1B). The behavior in different environments and interactions with organisms differs as well [18,19]. For instance, previously it has been found that chemically produced NPs are less toxic to soil ecosystems than those produced biologically. Conversely, only the chemically synthesized NPs provoked a marked proliferation of antibiotic-resistant bacteria, an effect comparable to that of ionic silver, whereas the biologically synthesized ones did not [59]. Similarly, AgNPs synthesized chemically and those produced biologically elicited distinct immune responses [60]. Furthermore, NPs derived from different microbial species triggered varied immunological profiles, underscoring their potential for targeted treatment of diseases. Servepali et al. [53] found that chemically synthesized AgNPs were more active against Gram-negative bacteria, while biologically synthesized were more active against Gram-positive bacteria. [52].

The type of AgNPs synthesis affects the NPs' properties and likely modulates the way each NPs type interacts with cellular light-harvesting systems and, ultimately, affects their phototoxic potential. Each synthesis pathway imprints a unique kinetic and chemical milieu on the nucleation and growth stages, dictating the final nanoparticle size distribution and morphology. According to [61], the toxicity of AgNPs to alga is primarily attributed to bioavailable dissolved silver, with particle size having little influence on photosynthetic inhibition. As all used NPs have a comparable size over 10 nm, direct penetration of the cell membrane is generally considered unlikely [31], with endocytosis or related uptake mechanisms being more probable [62]. However, differences in surface coating - such as the presence of protein-rich corona of biologically synthesized Agbio NPs - can affect the cellular uptake and potentially facilitate the passage through the multilayered cell walls [62], thus affecting their interaction with the alga. By contrast, the differently coated Agphys and Agchem NPs showed more modest effects on chlorophyll fluorescence (Figs. 2 and 4). Differences in surface chemistry and aggregation behavior may influence bioavailability: citrate-capped (Agchem) and surfactant-free polydisperse (Agphys) particles are prone to agglomeration in culture medium and may preferentially associate with the cell periphery rather than penetrate intracellularly [63], potentially resulting in reduced uptake and different toxicity kinetics compared to bio-corona-coated AgNPs. Notably, FLIM data showed a modest yet significant chlorophyll lifetime prolongation after 24 h exposure to Agchem and Agphys (Fig. 4), despite evidence of photosynthetic perturbation. Two non-mutually exclusive mechanisms may contribute to this observation, though both remain speculative without direct supporting measurements. First, partial inhibition of photochemical quenching pathways may temporarily prolong excited-state lifetimes. When PSII reaction centers are compromised—whether by nanoparticle interactions, released ions, or oxidative stress—the primary energy dissipation pathway is reduced. If this occurs faster than compensatory upregulation of non-photochemical quenching (NPQ) [64,65], transient accumulation of excited chlorophyll may manifest as modest lifetime increases. Second, surface-mediated stabilization effects cannot be excluded. In isolated systems, AgNPs have been reported to enhance chlorophyll photostability, potentially through interaction with the porphyrin ring [66,67], though the relevance of such in vitro observations to intact photosynthetic membranes remains uncertain. These interpretations are constrained by the absence of direct PSII activity measurements (e.g., PAM fluorometry), ROS quantification, or silver ion release kinetics, which would be required for definitive mechanistic conclusions.

Flavin fluorescence (500–550 nm, Fig. 5B) increased significantly at D1 for Agchem and Agphys ($p < 0.05$), with further elevation by D7, suggesting rapid oxidative perturbation of electron transport or flavoprotein redox state. In contrast, Agbio showed no significant D1 change, with elevation occurring only by D7. While flavins are redox-sensitive cofactors rather than direct ROS indicators, this temporal pattern may reflect differential kinetics driven by surface chemistry and capping agents. Citrate-capped and surfactant-free particles may mediate faster surface-driven oxidation [68], whereas bio-corona-coated Agbio may be more readily internalized, with the protein corona providing partial buffering against immediate stress and delaying intracellular

perturbation to later timepoints. Previous studies of biogenic, protein-capped AgNPs support this interpretation, demonstrating both immediate oxidative responsesand sustained upregulation of antioxidant systems, leading to long-term reductive adaptation [69–71].

All AgNP types depleted NAD(*P*)H photon counts at D1 (Fig. 6A), indicating rapid consumption of reducing equivalents, with severity ranking Agchem = Agphys > Agbio. By D7, Agchem and Agphys exhibited only partial metabolic recovery, remaining below control levels and suggesting chronic oxidative demand [72]. Agbio particles caused smaller initial depletion but showed notable partial rebound, implying early mobilisation of alternative reductive pathways [72,73]. Analysis of NAD(*P*)H lifetime amplitudes (a1/a2 ratio, Fig. 7) provided mechanistic insight into redox adaptation strategies. Agchem and Agphys significantly elevated a1/a2 at D1, indicating rapid shift toward oxidized state, with further elevation by D7 (increased a1, decreased a2), suggesting progressive depletion of reductive capacity. Conversely, Agbio showed no D1 change but decreased a_1/a_2 by D7 (decreased a1, increased a2), reflecting sustained mobilisation of bound (reduced) NAD(*P*)H [43,45]. The most pronounced, durable rise in both Tau1 and Tau2 NAD(*P*)H occurs with Agbio, corroborating earlier chlorophyll-FLIM and ROS data that flagged this formulation as the strongest intracellular stressor [73,74]. Changes in the a1 and a2 amplitudes of the NAD(*P*)H lifetimes suggest that cells, exposed to protein-coated Agbio particles, seem to massively deplete NADPH and likely channel into repair enzymes (e.g., glutathione and thioredoxin systems), building a long-term “reductive shield” against ongoing intracellular stress [68,73]. In contrast, Agchem is associated with a persistent deficit of reduced NAD(*P*)H, a_1/a_2 ratio and sustained oxidative stress, while Agphys induces a similar yet milder oxidative burden, as has previously been reported for other species [72].

Collectively, these data suggest synthesis-dependent, biphasic redox responses: weakly capped Agchem and Agphys particles elicit rapid, surface-driven oxidative perturbation with incomplete metabolic recovery, whereas bio-corona-coated particles (Agbio) induce delayed but more sustained intracellular stress coupled with greater compensatory reductive mobilisation. This framework parallels biphasic AgNP responses documented in bacteria [75] and mammalian cells [76], though our integrated fluorescence lifetime approach reveals synthesis-specific temporal dynamics not captured by conventional redox assays. Definitive mechanistic interpretation, however, requires complementary measurements of ROS production (e.g., fluorescent probes), nanoparticle uptake, silver ion release, pentose-phosphate pathway flux [77]), and NADPH/$NADP^+$ ratios [78].

Our integrated fluorescence-lifetime and redox analyses demonstrate that AgNP effects on *C. vulgaris* differ substantially depending on synthesis route. The observed temporal patterns—rapid surface-driven perturbation (Agchem/Agphys) versus delayed but sustained intracellular stress (Agbio)—suggest that physicochemical properties imparted by synthesis method, such as surface chemistry and capping agents, influence cellular interactions and redox response kinetics [35,79]. These findings support a biphasic redox framework: initial oxidative perturbation (evidenced by flavin elevation and NAD(*P*)H depletion at D1) followed by synthesis-dependent adaptation or persistent deficit (evidenced by differential a_1/a_2 dynamics by D7). While biphasic AgNP responses have been documented in bacteria and mammalian systems [75,76], our fluorescence lifetime approach reveals synthesis-specific temporal dynamics in photosynthetic microorganisms not captured by conventional redox assays [73].

However, this study has limitations that must be addressed in future work. The single-dose experimental design precludes quantitative toxicity ranking or determination of EC50. Comprehensive concentration-dependent studies are essential for establishing dose-response curves and enabling a robust comparative toxicity assessment across synthesis routes. Systematic variation of nanoparticle size within each synthesis method is also needed to differentiate size-dependent effects from surface chemistry contributions. Detailed molecular characterization of surface coatings would directly link specific physicochemical features to observed biological outcomes. Additional complementary biological endpoints, such as growth curves, viability assays, and direct photosynthetic efficiency measurements (e.g., PAM fluorometry), are required to validate the autofluorescence-based observations presented in this study. Finally, direct quantification of ROS production, nanoparticle cellular uptake, and silver ion release kinetics would be necessary to elaborate definitive mechanistic interpretations.

Gathered results underscore a critical principle: we cannot treat all silver nanoparticles as equivalent. The synthesis method must be considered an integral part of their functional and safety profile, with significant implications for environmental applications, therapeutic use, and nanosafety assessment [80,81]. Our study provides comparative proof-of-concept that integrated biochemical and optical imaging can refine nanotoxicological hazard assessments and guide a responsible AgNP deployment in environmental and biotechnological contexts. It underscores the importance of linking nanoparticle synthesis methods to their functional and safety profiles and highlights the value of integrated biochemical and imaging approaches in nanotoxicology to refine hazard assessments and support responsible deployment [73]. Although biphasic redox responses to AgNPs were previously noted in bacteria and mammalian cells, recent optical and metabolic studies refine this two-phase framework for photosynthetic microorganisms [[73], and this study]. These findings can be crucial for a comprehensive understanding of the interaction of NPs with living organisms and for guiding the responsible use of AgNPs in environmental and applied contexts.

Presented results demonstrate that AgNPs exercise a differential effect on the live alga based on their origin. Such complexity shows that we cannot treat all silver nanoparticles as equivalent. The synthesis method must therefore be considered an integral part of the AgNPs functional and safety profile. This finding has significant implications for the environmental applications, therapeutic use, and nanosafety.

5. Conclusion

AgNPs produced by the biological route (by living alga *P. kessleri* extract) were compared to those produced by the chemical approach (using Na citrate) vs. the physical approach (by laser ablation of Ag discs). Alga (*C. vulgaris*) was used as the model organism to study the biological effect of the produced AgNPs on organisms in aquatic ecosystems. Our observations indicate a significant impact of AgNPs produced through a biological route on the endogenous chlorophyll fluorescence of the alga. On the other hand, AgNPs produced by chemical or physical processes primarily affected algal metabolism, as evidenced by their impact on the flavin and/or NAD(*P*)H fluorescence.

Nevertheless, several factors need to be exploited in the future to understand the effect of nanoparticles in real ecosystems. Among the most important factors are surface chemistry variations (particularly the organic coronas formed during biological synthesis), size distribution differences, and colloidal stability, as well as variations in crystal structure and surface defects. The presence of biological reducing agents or stabilizers that remain associated with the AgNPs, as well as different aggregation behavior in biological media, also needs to be taken into consideration, together with concentration-dependent studies and testing of NPs of different sizes.

Understanding the interaction of NPs with living organisms is crucial for evaluating their potential environmental effects. AgNP/Ag^+ ions are considered the most toxic substance known to prokaryotic organisms. The protein coronas, aggregation behaviours, and surface chemistry emerging from different synthesis routes lead to a potential differential responsiveness of algal cells to AgNPs. Our contribution demonstrates that the production route can fundamentally alter the nanoparticle-biology interface.

CRediT authorship contribution statement

Alzbeta Marcek Chorvatova: Writing – review & editing, Writing – original draft, Investigation, Conceptualization. **Martin Uherek:** Investigation, Data curation. **Anton Mateasik:** Formal analysis, Data curation. **Jaroslav Bruncko:** Investigation. **Ildiko Matusikova:** Writing – review & editing, Writing – original draft. **Jana Sedlakova-Kadukova:** Writing – review & editing, Writing – original draft, Investigation, Conceptualization.

Consent for publication

All authors gave their consent for the ms to be published as submitted.

Ethical approval

No approval of research ethics committees was required to accomplish the goals of this study because experimental work was conducted with an unregulated invertebrate species. No patients participated in the presented research. Portions of the English editing (grammar and syntax) were assisted by ChatGPT (OpenAI, San Francisco, USA). The AI tool Grammarly was used for language, clarity and consistency.

Funding

Funded by the EU NextGenerationEU through the Recovery and Resilience Plan for Slovakia under the project ENVIROBIOM No 09I03-03-V04-00689, supported by VAIA and by the project VEGA 1/0785/26, supported by the Grant Agency of the Ministry of education, science, research and sport of the Slovak Republic.

Note: This work represents the continuation of recently completed project LASERLAB-EUROPE (grant agreement no. 871124, European Union's Horizon 2020 research and innovation programme) (A.MC.).

Declaration of competing interest

None beyond declared funding and affiliations.

Acknowledgements

The authors thank Dr. R. Hancinsky and Ing. P. Hlubina from FPV UCM for helping with the cultivation of *C. vulgaris*.

Data availability

Data are available at request in an Omero repository at http://microscopy.mlc.sk/omero.

References

[1] T. Jamatia, M.K. Das, R. Mazumder, Ichudaule, Floral extracts promising avenue for sustainable approach for nanoparticles: an updated review, Nanotechnol. Environ. Eng. 10 (2025) 26, https://doi.org/10.1007/s41204-025-00423-x.

[2] H. Duman, F. Eker, E. Akdaşçi, A.M. Witkowska, M. Bechelany, S. Karav, Silver nanoparticles: a comprehensive review of synthesis methods and chemical and physical properties, Nanomaterials 14 (18) (2024) 1527, https://doi.org/10.3390/nano14181527.

[3] A.S. Rodrigues, J.G.S. Batista, M.Á.V. Rodrigues, V.C. Thipe, L.A.R. Minarini, P. S. Lopes, A.B. Lugão, Advances in silver nanoparticles: a comprehensive review on their potential as antimicrobial agents and their mechanisms of action elucidated by proteomics, Front. Microbiol. 15 (2024) 1440065, https://doi.org/10.3389/fmicb.2024.1440065.

[4] A. Sati, T.N. Ranade, S.N. Mali, H.K. Ahmad Yasin, A. Pratap, Silver nanoparticles (AgNPs): comprehensive insights into bio/synthesis, key influencing factors, multifaceted applications, and toxicity—a 2024 update, ACS Omega 10 (8) (2025) 7549–7582, https://doi.org/10.1021/acsomega.4c11045.

[5] G.I. Edo, A.N. Mafe, A.B.M. Ali, P.O. Akpoghelie, E. Yousif, E.F. Isoje, U.A. Igbuku, K. Zainulabdeen, J.O. Owheruo, A.E.A. Essaghah, H. Umar, D.S. Ahmed, A. A. Alamiery, Eco-friendly nanoparticle phytosynthesis via plant extracts: mechanistic insights, recent advances, and multifaceted uses, Nano TransMed 4 (2025) 100080, https://doi.org/10.1016/j.ntm.2025.100080.

[6] V.K. Sharma, R.A. Yngard, Y. Lin, Silver nanoparticles: green synthesis and their antimicrobial activities, Adv. Colloid Interf. Sci. 145 (2009) 83–96, https://doi.org/10.1016/j.cis.2008.09.002.

[7] P. Peharec Štefanić, K. Košpić, D.M. Lyons, L. Jurković, B. Balen, M. Tkalec, Phytotoxicity of silver nanoparticles on tobacco plants: evaluation of coating effects on photosynthetic performance and chloroplast ultrastructure, Nanomaterials (Basel) 11 (3) (2021) 744, https://doi.org/10.3390/nano11030744. PMID: 33809644; PMCID: PMC8002358. Mar 16.

[8] J. Filipović Tričković, M. Momčilović, G. Joksić, S. Živković, B. Ilić, M. Ognjanović, M. Novaković, A. Valenta Šobot, Laser ablated citrate-stabilized silver nanoparticles display size and concentration dependant biological effects, Nanomater. Nanotechnol. 2023 (2023) 9854356, https://doi.org/10.1155/2023/9854356.

[9] E. Casals, T. Pfaller, A. Duschl, G.J. Oostingh, V.F. Puntes, Hardening of the nanoparticle–protein corona in metal (Au, Ag) and oxide (Fe3 O4, CoO, and CeO2) nanoparticles, Small 7 (2011) 3479–3486, https://doi.org/10.1002/smll.201101511.

[10] J. Wolfram, Y. Yang, J. Shen, A. Moten, C. Chen, H. Shen, M. Ferrari, Y. Zhao, The nano-plasma interface: implications of the protein corona, Colloids Surf. B Biointerfaces 124 (2014) 17–24, https://doi.org/10.1016/j.colsurfb.2014.02.035.

[11] S. Kumar, M. Kumar, V. Chauhan, D. Kaushal, Recent trends in the plant based metal oxide nanoparticles and their application in biomedical and waste water remediation - a review, Hybrid Adv. 10 (2025) 100475, https://doi.org/10.1016/j.hybadv.2025.100475.

[12] L. Xu, Y.-Y. Wang, J. Huang, C.-Y. Chen, Z.-X. Wang, H. Xie, Silver nanoparticles: synthesis, medical applications and biosafety, Theranostics 10 (2020) 8996–9031, https://doi.org/10.7150/thno.45413.

[13] R. Abbas, J. Luo, X. Qi, A. Naz, I.A. Khan, H. Liu, S. Yu, J. Wei, Silver nanoparticles: synthesis, structure, properties and applications, Nanomaterials 14 (2024) 1425, https://doi.org/10.3390/nano14171425.

[14] S. Ahmed, M. Ahmad, B.L. Swami, S. Ikram, A review on plants extract mediated synthesis of silver nanoparticles for antimicrobial applications: a green expertise, J. Adv. Res. 7 (2016) 17–28, https://doi.org/10.1016/j.jare.2015.02.007.

[15] G. Rana, V.K. Dhiman, S.K. Ali, A. Chauhan, M.S. Jabir, S. Ghotekar, Emerging developments in plant-based metal nanomaterials for diverse versatile applications - a review, Results Chem. 15 (2025) 102231, https://doi.org/10.1016/j.rechem.2025.102231.

[16] K. Deka, R.D. Nongbet, K. Das, P. Saikia, S. Kaur, A. Talukder, B. Thakuria, Understanding the mechanism underlying the green synthesis of metallic nanoparticles using plant extract(s) with special reference to silver, gold, copper and zinc oxide nanoparticles, Hybrid Adv. 9 (2025) 100399, https://doi.org/10.1016/j.hybadv.2025.100399.

[17] M. Bawskar, S. Deshmukh, S. Bansod, A. Gade, M. Rai, Comparative analysis of biosynthesised and chemosynthesised silver nanoparticles with special reference to their antibacterial activity against pathogens, IET Nanobiotechnol. 9 (2015) 107–113, https://doi.org/10.1049/iet-nbt.2014.0032.

[18] J. Kadukova, Surface sorption and nanoparticle production as a silver detoxification mechanism of the freshwater alga Parachlorella kessleri, Bioresour. Technol. 216 (2016) 406–413, https://doi.org/10.1016/j.biortech.2016.05.104.

[19] J. Kadukova, Surface sorption and nanoparticle production as a silver detoxification mechanism of the freshwater alga Parachlorella kessleri, Bioresour. Technol. 216 (2016) 406–413, https://doi.org/10.1016/j.biortech.2016.05.104.

[20] J. Sedlakova-Kadukova, O. Velgosova, M. Vosatka, J. Lukavsky, J. Dodd, J. Willner, A. Fornalczyk, Control over the biological synthesis of Ag nanoparticles by selection of the specific algal species, Arch. Metall. Mater. 62 (3) (2017) 1439–1442. ISSN 1733-3490, https://doi.org/10.1515/amm-2017-0222.

[21] L. Mikac, M. Ivanda, M. Gotić, T. Mihelj, L. Horvat, Synthesis and characterization of silver colloidal nanoparticles with different coatings for SERS application, J. Nanopart. Res. 16 (12) (2014) 2748, https://doi.org/10.1007/s11051-014-2748-92014/12/11.

[22] G. Yang. Laser Ablation in Liquids, Pan Stanford Publ., Singapore, 2012, p. 328, https://doi.org/10.1201/b11623.

[23] J. Kaduková, E. Virčíková, Comparison of differences between copper bioaccumulation and biosorption, Environ. Int. 31 (2) (2005) 227–232, https://doi.org/10.1016/j.envint.2004.09.020.

[24] A. Marcek Chorvatova, M. Uherek, A. Mateasik, D. Chorvat Jr., Time-resolved endogenous chlorophyll fluorescence sensitivity to pH: study on Chlorella sp. algae, Methods Appl. Fluoresc. 8 (2020) 024007, https://doi.org/10.1088/2050-6120/ab77f4.

[25] A. Marcek Chorvatova, A. Mateasik, D. Chorvat Jr., Differential effect of nano vs. micro-sized plastics on live *Chlorella* sp. algae in water environment, Microplastics Nanoplastics 5 (4) (2025) 1–9. SpringerNature, https://doi.org/10.1186/s43591-025-00111-2.

[26] J. Bruncko, M. Michalka, J. Kovac, et al., A low-temperature limit for growth of ZnO nanowires by using of laser ablation processes, Appl. Phys. A Mater. Sci. Process. 126 (2020) 305, https://doi.org/10.1007/s00339-020-03477-7.

[27] N. Otsu, A threshold selection method from gray-level histograms, IEEE Transactions on Systems, Man, and Cybernetics 9 (1) (1979) 62–66, https://doi.org/10.1109/TSMC.1979.4310076.

[28] A. Syafiuddin, S. Salmiati, T. Hadibarata, et al., Silver nanoparticles in the water environment in Malaysia: inspection, characterization, removal, modeling, and future perspective, Sci. Rep. 8 (2018) 986, https://doi.org/10.1038/s41598-018-19375-1.

[29] H. Kong, J. Jang, One-step fabrication of silver nanoparticle embedded polymer nanofibers by radical-mediated dispersion polymerization, Chem. Commun. (2006) 3010–3012, https://doi.org/10.1039/B605286J.

[30] C. Petit, P. Lixon, M.-P. Pileni, In situ synthesis of silver nanocluster in AOT reverse micelles, J. Phys. Chem. 97 (1993) 12974–12983, https://doi.org/10.1021/j100151a054.

[31] O. Choi, K.K. Deng, N.-J. Kim, L. Ross, R.Y. Surampalli, Z. Hu, The inhibitory effects of silver nanoparticles, silver ions and silver chloride colloids on microbial growth, Water Res. 42 (2008) 3066–3074, https://doi.org/10.1016/j.watres.2008.02.021.

[32] W.F. Falco, A.M. Queiroz, J. Fernandes, E.R. Botero, E.A. Falcão, F.E.G. Guimarães, J.-C. M'Peko, S.L. Oliveira, I. Colbeck, A.R.L. Caires, Interaction between chlorophyll and silver nanoparticles: a close analysis of chlorophyll fluorescence quenching, J. Photochem. Photobiol. A Chem. 299 (2015) 203–209, https://doi.org/10.1016/j.jphotochem.2014.12.001.

[33] M.F. Hohmann-Marriott, K. Takizawa, J.J. Eaton-Rye, L. Mets, J. Minagawa, The redox state of the Plastoquinone Pool directly modulates minimum chlorophyll fluorescence yield in *Chlamydomonas reinhardtii*, FEBS Lett. 584 (5) (2010) 1021–1026, https://doi.org/10.1016/j.febslet.2010.01.052.

[34] C. Carlson, S.M. Hussain, A.M. Schrand, L.K. Braydich-Stolle, K.L. Hess, R.L. Jones, J.J. Schlager, Unique cellular interaction of silver nanoparticles: size-dependent generation of reactive oxygen species, J. Phys. Chem. B 112 (43) (2008) 13608–13619, https://doi.org/10.1021/jp712087m. Oct 30.

[35] B. Komazec, P. Cvjetko, B. Balen, I. Letofsky-Papst, D.M. Lyons, Štefanić P. Peharec, The occurrence of oxidative stress induced by silver nanoparticles in Chlorella vulgaris depends on the surface-stabilizing agent, Nanomaterials 13 (2023) 1967, https://doi.org/10.3390/nano13131967.

[36] J. Zhang, L. Shen, Q. Xiang, J. Ling, C. Zhou, J. Hu, L. Chen, Proteomics reveals surface electrical property-dependent toxic mechanisms of silver nanoparticles in Chlorella vulgaris, Environ. Pollut. 265 (2020) 114743, https://doi.org/10.1016/j.envpol.2020.114743.

[37] A. Marcek Chorvatova, M. Cagalinec, D. Chorvat Jr., Time-resolved imaging of mitochondrial Flavin fluorescence and its applications for evaluating the oxidative state in living cardiac cells, in: V. Weissig, M. Edeas (Eds.), mitochondrial medicine, Methods in molecular biology, 2275, Humana, New York, NY, 2021, pp. 403–414, volume 1: targeting mitochondria. ISBN 978-1-0716-1262-0, https://doi.org/10.1007/978-1-0716-1262-0_26.

[38] S. White, A. Anandraj, C. Trois, NADPH fluorescence as an indicator of hydrogen production in the green algae Chlamydomonas reinhardtii, Int. J. Hydrog. Energy 39 (4) (2014) 1640–1647, https://doi.org/10.1016/j.ijhydene.2013.11.016.

[39] H. Kumar, K. Bhardwaj, E. Nepovimova, K. Kuča, D. Dhanjal, S. Bhardwaj, S. Bhatia, R. Verma, D. Kumar, Antioxidant functionalized nanoparticles: a combat against oxidative stress, Nanomaterials 10 (2020), https://doi.org/10.3390/nano10071334.

[40] Y. Wang, Y. Lee, C. Chou, Y. Chang, W. Liu, H. Chiu, Oxidative stress and potential effects of metal nanoparticles: a review of biocompatibility and toxicity concerns, Environ. Pollut. (2024) 123617, https://doi.org/10.1016/j.envpol.2024.123617.

[41] T. Blacker, Z. Mann, J. Gale, et al., Separating NADH and NADPH fluorescence in live cells and tissues using FLIM, Nat. Commun. 5 (2014) 3936, https://doi.org/10.1038/ncomms4936.

[42] T. Blacker, T. Berecz, M. Duchen, G. Szabadkai, Assessment of cellular redox state using NAD(P)H fluorescence intensity and lifetime, Bio-protocol 7 (2017) 2, https://doi.org/10.21769/BioProtoc.2105.

[43] R. Cao, H. Wallrabe, K. Siller, S. Alam, A. Periasamy, Single-cell redox states analyzed by fluorescence lifetime metrics and tryptophan FRET interaction with NAD(P)H, Cytometry A 95 (2019), https://doi.org/10.1002/cyto.a.23711.

[44] A. Chorvatova, S. Aneba, A. Mateasik, D. Chorvat Jr., B. Comte, Time-resolved fluorescence spectroscopy investigation of the effect of 4-hydroxynonenal on endogenous NAD(P)H in living cardiac myocytes, J. Biomed. Opt. 18 (6) (2013), https://doi.org/10.1117/1.JBO.18.6.067009, 067009-1-11.

[45] H. Wallrabe, Z. Svindrych, S. Alam, K. Siller, T. Wang, D. Kashatus, S. Hu, A. Periasamy, Segmented cell analyses to measure redox states of autofluorescent NAD(P)H, FAD & Trp in cancer cells by FLIM, Sci. Rep. 8 (2018), https://doi.org/10.1038/s41598-017-18634-x.

[46] M. Oćwieja, A. Barbasz, M. Wasilewska, P. Smoleń, D. Duraczyńska, B. Napruszewska, M. Kozak, A. Węgrzynowicz, Surface charge-modulated toxicity of cysteine-stabilized silver nanoparticles, Molecules 29 (2024), https://doi.org/10.3390/molecules29153629.

[47] B. Vuković, M. Milić, B. Dobrošević, M. Milić, K. Ilić, I. Pavičić, V. Šerić, I. Vrček, Surface stabilization affects toxicity of silver nanoparticles in human peripheral blood mononuclear cells, Nanomaterials 10 (2020), https://doi.org/10.3390/nano10071390.

[48] L. Ahmed, M. Milić, I. Pongrac, A. Marjanović, H. Mlinarić, I. Pavičić, S. Gajović, V. Vrček, Impact of surface functionalization on the uptake mechanism and toxicity effects of silver nanoparticles in HepG2 cells, Food and chemical toxicology: an international journal published for the British Industrial Biological Research Association 107 Pt A (2017) 349–361, https://doi.org/10.1016/j.fct.2017.07.016.

[49] S.C. Kulkarni, V.T. Salunke, S. Naeem, A.V. Patil, M. Shaheer Akhtar, S. Ameen, Sustainable synthesis of indium oxide nanoparticles via aloe Vera for gas sensing applications, Microchem. J. 207 (2024) 111941, https://doi.org/10.1016/j.microc.2024.111941.

[50] O.A. Carrasco-Jaim, R. Ahumada-Lazo, P.C.J. Clark, C. Gómez-Solis, S. M. Fairclough, S.J. Haigh, M.A. Leontiadou, K. Handrup, L.M. Torres-Martínez, W. R. Flavell, Photocatalytic hydrogen production by biomimetic indium sulfide using Mimosa pudica leaves as template, Int. J. Hydrog. Energy 44 (2019) 2770–2783, https://doi.org/10.1016/j.ijhydene.2018.12.043.

[51] B. Calderón-Jiménez, A. Bustos, R. Reyes, S. Paniagua, J. Vega-Baudrit, Novel pathway for the sonochemical synthesis of silver nanoparticles with near-spherical shape and high stability in aqueous media, Sci. Rep. 12 (2022), https://doi.org/10.1038/s41598-022-04921-9.

[52] C.H.N. de Barros, G.C.F. Cruz, W. Mayrink, L. Tasic, Bio-based synthesis of silver Nanoparticles from Orange waste: effects of distinct biomolecule coatings on size, morphology, and antimicrobial activity, Nanotechnol. Sci. Appl. 11 (2018) 1–14, https://doi.org/10.2147/NSA.S156115.

[53] M. Sarvepalli, A. Velidandi, N. Korrapati, Chemical vs biological silver nanoparticles: synthesis, characterization, properties, and *in vitro* applications, Inorg. Chem. Commun. 167 (2024) 112667, https://doi.org/10.1016/j.inoche.2024.112667.

[54] B. Dong, N. Xue, G. Mu, M. Wang, Z. Xiao, L. Dai, Z. Wang, D. Huang, H. Qian, W. Chen, Synthesis of monodisperse spherical AgNPs by ultrasound-intensified Lee-Meisel method, and quick evaluation via machine learning, Ultrason. Sonochem. 73 (2021), https://doi.org/10.1016/j.ultsonch.2021.105485.

[55] H.M. Abdelmigid, M.M. Morsi, N.A. Hussien, A.A. Alyamani, N.M. Al Sufyani, Comparative analysis of Nanosilver particles synthesized by different approaches and their antimicrobial efficacy, J. Nanomater. 2021 (2021) 2204776, https://doi.org/10.1155/2021/2204776.

[56] M. Asif, R. Yasmin, R. Asif, A. Ambreen, M. Mustafa, S. Umbreen, Green synthesis of silver nanoparticles (AgNPs), structural characterization, and their antibacterial potential, Dose-Response 20 (2022), https://doi.org/10.1177/15593258221088709.

[57] N. GöktürkBaydar, Z. Babalık, T. Demirci, A. Cessur, Synthesis methods impact silver nanoparticle properties and phenolic compound production in grapevine cell cultures, Sci. Rep. 15 (2025), https://doi.org/10.1038/s41598-025-85545-7.

[58] A. Miškovská, M. Rabochová, J. Michailidu, J. Masák, A. Čejková, J. Lorinčík, O. Maťátková, Antibiofilm activity of silver nanoparticles biosynthesized using Viticultural waste, PloS One 17 (8) (2022) e0272844, https://doi.org/10.1371/journal.pone.0272844.

[59] J. Sedlakova-Kadukova, M. Sincak, V. Demčakova, Does the silver nanoparticles production route affect the proliferation of antibiotic resistance in soil ecosystem? Antibiotics 14 (2024) 15, https://doi.org/10.3390/antibiotics14010015.

[60] V. Demeckova, V. Demcakova, J. Sedlakova-Kadukova, Differences in immunological impact of chemically and biologically synthesized silver nanoparticles, IEEE Trans. Nanobioscience (2025) 434–442, https://doi.org/10.1109/TNB.2025.3564822.

[61] E. Navarro, B. Wagner, N. Odzak, L. Sigg, R. Behra, Effects of differently coated silver nanoparticles on the photosynthesis of Chlamydomonas reinhardtii, Environ. Sci. Technol. 49 (13) (2015), https://doi.org/10.1021/acs.est.5b01089, 8041–7. Jul 7. Epub 2015 Jun 8. PMID: 26018638.

[62] X. Zhang, W. Shen, S. Gurunathan, Silver nanoparticle-mediated cellular responses in various cell lines: an in vitro model, Int. J. Mol. Sci. 17 (2016), https://doi.org/10.3390/ijms17101603.

[63] P. Štefanić, K. Košpić, D. Lyons, L. Jurković, B. Balen, M. Tkalec, Phytotoxicity of silver nanoparticles on tobacco plants: evaluation of coating effects on photosynthetic performance and chloroplast ultrastructure, Nanomaterials 11 (2021), https://doi.org/10.3390/nano11030744.

[64] V. Mays, N. Smith, C. Pham, M. White, Q. Wu, J. Berry, A. Linan, A. Wait, L. Kovacs, Attenuation of photosynthesis in nanosilver-treated *Arabidopsis thaliana* is inherently linked to the particulate nature of silver, Heliyon 10 (2024), https://doi.org/10.1016/j.heliyon.2024.e27583.

[65] A. Rastogi, M. Živčák, D. Tripathi, S. Yadav, H. Kalaji, Phytotoxic effect of silver nanoparticles in *Triticum aestivum*: improper regulation of photosystem I activity as the reason for oxidative damage in the chloroplast, Photosynthetica (2019), https://doi.org/10.32615/PS.2019.019.

[66] L. Bekalé, S. Barazzouk, S. Hotchandani, Nanosilver could usher in next-generation Photoprotective agents for magnesium porphyrins, Part. Part. Syst. Charact. 31 (8) (2014) 843–850, https://doi.org/10.1002/ppsc.201400008.

[67] A.M. Queiroz, A.V. Mezacasa, D.E. Graciano, W.F. Falco, J.C. M'Peko, F.E. G. Guimarães, T. Lawson, I. Colbeck, S.L. Oliveira, A.R.L. Caires, Quenching of chlorophyll fluorescence induced by silver nanoparticles, Spectrochim. Acta A Mol. Biomol. Spectrosc. 5 (168) (2016) 73–77, https://doi.org/10.1016/j.saa.2016.05.033. Nov. Epub 2016 May 25. PMID: 27280858.

[68] R. Biba, P. Cvjetko, M. Tkalec, K. Košpić, P.P. Štefanić, S. Šikić, A.-M. Domijan, B. Balen, Effects of silver nanoparticles on physiological and proteomic responses of tobacco (*Nicotiana tabacum*) seedlings are coating-dependent, Int. J. Mol. Sci. 23 (24) (2022) 15923, https://doi.org/10.3390/ijms232415923.

[69] P. Bustos, M. Quinteros, D. Gomez, M. Ortega, P. Páez, N. Guiñazú, Silver bionanoparticles toxicity in trophoblast is mediated by nitric oxide and glutathione pathways, Toxicology (2021) 152741, https://doi.org/10.1016/j.tox.2021.152741.

[70] S. Gurunathan, M. Qasim, C. Park, H. Yoo, J. Kim, K. Hong, Cytotoxic potential and molecular pathway analysis of silver nanoparticles in human Colon Cancer cells HCT116, Int. J. Mol. Sci. 19 (2018), https://doi.org/10.3390/ijms19082269.

[71] M. Wypij, T. Jędrzejewski, J. Trzcińska-Wencel, M. Ostrowski, M. Rai, P. Golińska, Green synthesized silver nanoparticles: antibacterial and anticancer activities, biocompatibility, and analyses of surface-attached proteins, Front. Microbiol. 12 (2021) 632505, https://doi.org/10.3389/fmicb.2021.632505.

[72] T. Ameh, M. Gibb, D. Stevens, S. Pradhan, E. Braswell, C. Sayes, Silver and copper nanoparticles induce oxidative stress in Bacteria and mammalian cells, Nanomaterials 12 (2022), https://doi.org/10.3390/nano12142402.

[73] W. Liu, S. Majumdar, W. Li, A. Keller, V. Slaveykova, Metabolomics for early detection of stress in freshwater alga Poterioochromonas malhamensis exposed to

silver nanoparticles, Sci. Rep. 10 (2020), https://doi.org/10.1038/s41598-020-77521-0.
[74] R.Y. Prasad, J.K. McGee, M.G. Killius, D.A. Suarez, C.F. Blackman, D.M. DeMarini, S.O. Simmons, Investigating oxidative stress and inflammatory responses elicited by silver nanoparticles using high-throughput reporter genes in HepG2 cells: effect of size, surface coating, and intracellular uptake, Toxicol. in Vitro 27 (6) (2013) 2013–2021, https://doi.org/10.1016/j.tiv.2013.07.005.
[75] A. Ivask, I. Kurvet, K. Kasemets, I. Blinova, V. Aruoja, S. Suppi, H. Vija, A. Käkinen, T. Titma, M. Heinlaan, M. Visnapuu, D. Koller, V. Kisand, A. Kahru, Size-dependent toxicity of silver nanoparticles to bacteria, yeast, algae, crustaceans and mammalian cells in vitro, PLoS One 9 (7) (2014), https://doi.org/10.1371/journal.pone.0102108 e102108. Jul 21. PMID: 25048192; PMCID: PMC4105572.
[76] A. Onodera, F. Nishiumi, K. Kakiguchi, A. Tanaka, N. Tanabe, A. Honma, K. Yayama, Y. Yoshioka, K. Nakahira, S. Yonemura, I. Yanagihara, Y. Tsutsumi, Y. Kawai, Short-term changes in intracellular ROS localisation after the silver nanoparticles exposure depending on particle size, Toxicol. Rep. 23 (2) (2015) 574–579, https://doi.org/10.1016/j.toxrep.2015.03.004.
[77] L. de Freitas-Silva, M. Rodríguez-Ruiz, H. Houmani, L.C. da Silva, J.M. Palma, F. J. Corpas, Glyphosate-induced oxidative stress in *Arabidopsis thaliana* affecting Peroxisomal metabolism and triggers activity in the oxidative phase of the pentose phosphate pathway (OxPPP) involved in NADPH generation, J. Plant Physiol. 218 (2017) 196–205, https://doi.org/10.1016/j.jplph.2017.08.007.
[78] X. Zou, P. Li, J. Lou, H. Zhang, Surface coating-modulated toxic responses to silver nanoparticles in *Wolffia globosa*, Aquat. Toxicol. 189 (2017) 150–158, https://doi.org/10.1016/j.aquatox.2017.06.010.
[79] R. Abo-Elmagd, R. Hamouda, M. Hussein, Phycotoxicity and catalytic reduction activity of green synthesized Oscillatoria gelatin-capped silver nanoparticles, Sci. Rep. 12 (2022), https://doi.org/10.1038/s41598-022-22976-6.
[80] D. Chugh, V. Viswamalya, B. Das, Green synthesis of silver nanoparticles with algae and the importance of capping agents in the process, J. Genet. Eng. Biotechnol. 19 (2021), https://doi.org/10.1186/s43141-021-00228-w.
[81] R. Hamida, M. Ali, M. Alkhateeb, H. Alfassam, M. Momenah, M. Bin-Meferij, Harnessing Desmochloris edaphica strain CCAP 6006/5 for the eco-friendly synthesis of silver nanoparticles: insights into the anticancer and antibacterial efficacy, Molecules 29 (2024), https://doi.org/10.3390/molecules29163750.
[82] Y. Balmer, W.H. Vensel, C.K. Tanaka, W.J. Hurkman, E. Gelhaye, N. Rouhier, J.-P. Jacquot, W. Manieri, P. Schürmann, M. Droux, B.B. Buchanan, Thioredoxin links redox to the regulation of fundamental processes of plant mitochondria, Proc. Natl. Acad. Sci. USA 101 (8) (2004) 2642–2647, https://doi.org/10.1073/pnas.0308583101.